0 0 0 0 4 9 0 0 8 8 8

uc-4
uc-90d

LBL-6842 c.1

To be presented at the Fall Meeting of the Western States Section of the Combustion Institute, Stanford, CA, October 17 - 18, 1977

RECEIVED
LAWRENCE
BERKELEY LABORATORY

OCT 18 1977

LIBRARY AND
DOCUMENTS SECTION

For Reference

Not to be taken from this room

Energy and Environment Division

Catalyzed Combustion in a Flat Plate Boundary Layer II. Numerical Calculations

R. Schefer and F. Robben

September 1977

Lawrence Berkeley Laboratory University of California/Berkeley

Prepared for the U.S. Energy Research and Development Administration under Contract No. W-7405-ENG-48

LBL-6842 c.1

LEGAL NOTICE

This report was prepared as an account of work sponsored by the United States Government. Neither the United States nor the Department of Energy, nor any of their employees, nor any of their contractors, subcontractors, or their employees, makes any warranty, express or implied, or assumes any legal liability or responsibility for the accuracy, completeness or usefulness of any information, apparatus, product or process disclosed, or represents that its use would not infringe privately owned rights.

0 0 0 0 4 9 0 0 8 8 9

CATALYZED COMBUSTION IN A FLAT PLATE BOUNDARY LAYER
II. NUMERICAL CALCULATIONS[†*]

R. Schefer[++] and F. Robben

September 1977

[†]To be presented at the Fall Meeting, Western States Section of the Combustion Institute, October 17-18 Stanford, California

*This work was primarily supported by ERDA, Division of Conservation Research and Technology. The experimental equipment and technique were jointly supported by the Air Force Office of Scientific Research and ERDA, Division of Basic Energy Sciences.

[++]NSF Energy Related Postdoctoral Fellow

0 0 3 0 4 9 0 0 8 9 0

Abstract

A computer program has been developed to solve the boundary layer equations for laminar flow over a heated plate with H_2/air combustion. The objectives are to investigate the importance of homogeneous as opposed to catalytic surface reactions during the combustion process, and to determine the roles of heat and mass transfer and their effect on combustion. Results are presented for combustion of H_2/air at an equivalence ratio of 0.1 for flow over a noncatalytic plate at a surface temperature of 1100 K. A detailed mechanism involving 8 chemical species and 13 reactions has been used to describe the kinetics. The reactions leading to the initiation of combustion and the effect of the large diffusivity of hydrogen are discussed. The boundary conditions for a catalytic surface and a simplified model to account for catalytic wall reaction are formulated. Results are presented for combustion over a catalytic surface and compared with the non-catalytic case.

INTRODUCTION

Interest in the use of catalytic surfaces to promote combustion reactions has increased greatly over the past several years. A number of studies have been undertaken which indicate that catalytically supported combustion makes efficient burning of a variety of fuels possible under fuel lean conditions with a substantial reduction in NO_x levels.[1,2] While initial emphasis was based on the use of catalytic combustors for aircraft gas turbine application[1,3] its potential application to stationary power sources has also been studied with favorable results.[4]

Much of the work to date has involved parametric investigations of prototype catalytic combustor configurations. The results of such studies are both necessary to the long term development of catalytic combustors and have been very promising. However, such studies are somewhat limited in terms of deriving an understanding of catalytically supported combustion. Two such areas where a greater knowledge would be desirable are the role of internal heat and mass transfer in the catalytic combustion process, and the role of homogeneous as opposed to catalytic surface reactions during the combustion process. An understanding of these and related processes is necessary for the optimum evaluation and application of the catalytic concept to practical combustion system design.

0 0 0 0 4 9 0 0 8 9 1

An experimental and theoretical investigation has been undertaken of combustion over heated noncatalytic and catalytic flat plates. Such a system is desireable from the standpoint of the simplified geometry and the relatively well characterized flowfield it provides. As part of this study a computer program has been developed to solve the boundary layer equations for flow over a heated plate with H_2/air combustion. Comparisons with experimental results over a noncatalytic surface are made in a companion paper[5] to verify the model. In the present paper the model and numerical procedure are discussed. A detailed reaction mechanism involving 8 species and 13 reactions is used in the program to examine the development of the combustion process along the plate boundary layer. Results are presented for the combustion of H_2/air at an equivalence ratio of 0.1 over a heated noncatalytic plate with a wall temperature of 1100 K. Observations are made concerning the role of kinetics and the importance of realistic transport properties. In the final section the boundary conditions for a catalytic surface are formulated, and a model for surface ctatlyzed reaction rates, taking into account both forward and reverse reactions, is discussed. Results for combustion over a catalytic surface are presented and discussed.

NUMERICAL MODEL FOR BOUNDARY LAYER COMBUSTION

Governing Equations

The boundary layer equations for laminar flow over a flat plate of a multicomponent mixture of chemically reacting gases can be written as follows:

Continuity equation

$$\frac{\partial}{\partial x}(\rho u) + \frac{\partial}{\partial y}(\rho v) = 0 \tag{1}$$

Momentum equation

$$\rho u\frac{\partial u}{\partial x} + \rho v\frac{\partial u}{\partial y} = \frac{\partial}{\partial y}(\mu\frac{\partial u}{\partial y}) + \rho g\beta(T - T_\infty) \tag{2}$$

Energy equation

$$\rho u\frac{\partial h}{\partial x} + \rho v\frac{\partial h}{\partial y} = \frac{\partial}{\partial y}\left\{\frac{\mu}{Pr}\left[\frac{\partial h}{\partial y} + \sum_i h_i(Le_i - 1)\frac{\partial \sigma_i}{\partial y}\right]\right\} + \mu(\frac{\partial u}{\partial y})^2 \tag{3}$$

Species equation

$$\rho u\frac{\partial \sigma_i}{\partial x} + \rho v\frac{\partial \sigma_i}{\partial y} = -\frac{\partial}{\partial y}\left\{\sum_i Le_i\frac{\partial \sigma_i}{\partial y}\right\} + S_{kinetic} \tag{4}$$

Also, assuming ideal gas behavior, the equation of state provides an additional relation

$$\rho = \frac{P}{RT} \tag{5}$$

The diffusion coefficients used to evaluate the Lewis number in Eq. (3) are trace diffusion coefficients for the ith specie in N_2. Actual diffusion coefficients which are a function of mixture composition and the

binary diffusion coefficients of all species pairs. However, since the principle constituent in the present system is N_2, trace diffusion coefficients were used to simplify the calculations[6]. Equations (1) through (5) form a set of NS + 4 equations for the dependent variables u, v, h, ρ, and σ_i (i - 1, NS)

Introducing the similarity variables

$$\xi(x) = (\rho\mu)_\infty U_\infty X$$

$$\eta(x,y) = \frac{U_\infty}{\eta_e\sqrt{2\xi}} \int_0^y \rho dy \tag{6}$$

considerably simplifies the numerical computations. The governing equations (1) through (4) then become

Continuity equation

$$2\xi\frac{\partial f'}{\partial \xi} + \frac{1}{\eta_e}\frac{\partial f'}{\partial \eta} + f' = 0 \tag{7}$$

Momentum equation

$$2\xi f'\frac{\partial f'}{\partial \xi} + (V - \ell')\frac{1}{\eta_e^2}\frac{\partial f'}{\partial \eta} = \frac{1}{\eta_e^2}\frac{\partial^2 f'}{\partial \eta^2} + \frac{e}{U_\infty} g\beta(T - T_\infty) \tag{8}$$

Energy equation

$$2\xi f'\frac{\partial h}{\partial \xi} + (V - \frac{\bar{c}'}{c_p})\frac{1}{\eta_e}\frac{\partial h}{\partial \eta} - \frac{\ell U_e^2}{\eta_e^2}(\frac{\partial f'}{\partial \eta})^2 - \frac{\bar{c}}{\eta_e c_p}(\frac{\partial^2 h}{\partial \eta^2})$$

$$= \frac{1}{(\rho\mu)_\infty \eta_e^2}\frac{\partial}{\partial \eta}\left[\frac{k\rho}{c_p}\sum_i (Le_i - 1)h_i\frac{\partial \sigma_i}{\partial \eta}\right] \tag{9}$$

Species equation

$$2\xi f'\frac{\partial\sigma_i}{\partial\xi} + (V - b_i')\frac{1}{\eta_e}\frac{\partial\sigma_i}{\partial\eta} - \frac{b_i}{\eta_e^2}\frac{\partial^2\sigma_i}{\partial\eta^2} - \frac{e}{\rho}S_{\sigma i} = 0 \qquad (10)$$

The following dimensionless quantities have been introduced:

$$V = \frac{2\xi}{(\rho\mu)_\infty U_\infty}\left(f'\frac{\partial\eta}{\partial x} + \frac{\rho v}{\sqrt{2\xi}}\right)$$

$$\bar{c} = \frac{l\bar{c}p}{Pr} \quad ; \quad b_i = \frac{\ell Le_i}{Pr}$$

$$\ell = \frac{\rho\mu}{(\rho\mu)_\infty} \quad ; \quad f' = \frac{u}{u_\infty}$$

$$e = \frac{2\xi}{U_\infty\left(\frac{d\xi}{dx}\right)} \quad ;$$

η_e represents the value of η at the outer edge of the boundary layer.

Boundary Condition

Boundary conditions are required at the wall and at the edge of the boundary layer. In the present case these are given for velocity and enthalpy at the wall as

$$f'(\xi,0) = 0 \quad ; \quad h(\xi,0) = h_w(x) \qquad (11)$$

The species boundary condition depends on whether the wall is non-catalytic or catalytic. For a non-catalytic wall

$$\frac{\partial}{\partial\eta}(\sigma_i)\Big|_w = 0 \tag{12}$$

Boundary conditions at the outer edge of the boundary layer for the dependent variables are given by the following:

$$f'(\xi,\eta_e) = 1 \quad ; \quad h(\xi,\eta_e) = h_\infty$$

$$\sigma_i(\xi,\eta_e) = \sigma_{i\infty} \tag{13}$$

where free stream conditons are assumed to be constant along the plate. A value for η_e of 9.0 was found sufficient in the present calculations.

Gas Properties

The mixutre viscosity and thermal conductivity are calculated from single component transport properties using the semi-empirical expression of Wilke [7]

$$\mu = \sum_{i=1}^{ms} \frac{X_i \mu_i}{\sum_{j=1}^{ms} X_j \Phi_{ij}} \tag{14}$$

and

$$k = \sum_{i=1}^{ms} \frac{X_i k_i}{\sum_{j=1}^{ms} X_j \Phi_{ij}} \tag{15}$$

where

$$\Phi_{ij} = \frac{1}{\sqrt{8}}\left(1 + \frac{M_i}{M_j}\right)^{-\frac{1}{2}}\left[1 + \left(\frac{\mu}{\mu_j}\right)^{\frac{1}{2}}\left(\frac{M_j}{M_i}\right)^{\frac{1}{4}}\right]^2$$

Single component properties μ_i, and the binary diffusion coefficients D_{ij} were calculated from the Chapman-Enskog theory[7] where

$$\mu_i = 2.6693 \times 10^{-5} \frac{(M_i T)^{\frac{1}{2}}}{\sigma_i^2 \Omega_\mu^{(2,2)}} \tag{16}$$

$$D_{ij} = \frac{0.01883\left(\frac{1}{Mi} + \frac{1}{Mj}\right)^{\frac{1}{2}} T^{\frac{3}{2}}}{p\sigma_{ij}^2 \Omega_{ij}^{(1,1)}} \tag{17}$$

The molecular parameters σ and ε/k and the collision integrals $\Omega^{(2,2)}$ and $\Omega_{i,j}^{(1,1)}$ were evaluated using a Lennard Jones potential model[8]. The single component thermal conductivity was evaluated from viscosity data using the modified Euken correction[6]

$$k = (0.4312R + 1.328C_{pi})\frac{\mu_i}{M_i} \tag{18}$$

Expected errors in using the above equations to predict viscosity and thermal conductivity are on the order of 2% for nonpolar molecules and 5% for polar molecules and radicals. The general lack of diffusivity data at higher temperatures means that molecular parameters must be estimated from viscosity data. The resulting discrepancy can range from within 5% at room temperature to 20% as 2000K is approached for some species.

The thermodynamic data for specific heat and enthalpy were calculated from JANAF data using a formalism based on the NASA Complex Chemical Equilibrium Code[9].

Chemical Kinetics

The general set of reactions occurring in the system can be written for the ith reaction as

$$\sum_{i=1}^{mr} \alpha_{ij}\sigma_i + \bar{\alpha}_j M \quad \sum_{i=1}^{mr} \alpha_{ij}\sigma_i + \bar{\alpha}_j M \ , \quad j = 1,2...T$$

where α_{ij} is the stoichiometric coefficient for the ith species in the ith reaction and $\bar{\alpha}_j$ is the stoiciometric coefficient of the third body M. The forward and reverse reaction rates of the ith reaction can be written

$$R_j = k_j (\rho\sigma_m)^{\bar{\alpha}_j} \prod_{i=1}^{NS} (\rho\sigma_i)^{\alpha'_{ij}} \ , \quad j = 1,2...J$$

$$R_{-j} = k_{-j} (\rho\sigma_m)^{\bar{\alpha}_j} \prod_{i=1}^{NS} (\rho\sigma_i)^{\alpha''_{ij}} \ , \quad j = 1,2...J$$

k_j is an Arrhenius rate coefficient of the form

$$k_j = 10^{B_j} T^{N_j} \exp\ (-E_j/RT).$$

Reverse rate coefficients were assumed to be related to the forward rate constants through the equilibrium constant K_{cj}

TABLE I

H_2 - Air Reaction Mechanism

	Reaction	k	Ref.
1.	$O + H_2 \rightleftarrows OH + H$	$10^{7.255} T^{1.0} \exp(-4479.0/T)$	7
2.	$H_2 + OH \rightleftarrows H_2O + H$	$10^{10.35} \exp(-2617.0/T)$	8
3.	$H + O_2 \rightleftarrows O + OH$	$10^{11.342} \exp(-8450.0/T)$	9
4.	$OH + OH \rightleftarrows H_2O + O$	$10^{9.800} \exp(-550.0/T)$	9
5.	$H_2 + M \rightleftarrows H + H + M$	$10^{9.348}\ T^{0.5} \exp(-48414.0/T)$	20
6.	$H + OH + M \rightleftarrows H_2O + M$	$10^{16.342}\ T^{-2.0}$	19
7.	$O + O + M \rightleftarrows O_2 + M$	$10^{11.410}\ T^{-1.0} \exp(-171.5/T)$	21
8.	$H + O_2 + M \rightleftarrows HO_2 + M$	$10^{9.350} \exp(500.0/T)$	19
9.	$HO_2 + H \rightleftarrows OH + OH$	$10^{11.400} \exp(-950.0/T)$	19
10.	$HO_2 + OH \rightleftarrows H_2O + O_2$	$10^{10.699} \exp(-503.3/T)$	22
11.	$HO_2 + O \rightleftarrows OH + O_2$	$10^{10.699} \exp(-503.3/T)$	22
12.	$HO_2 + H \rightleftarrows H_2O + O$	$10^{10.699} \exp(-503.3/T)$	22
13.	$HO_2 + H \rightleftarrows H_2 + O_2$	$10^{10.398} \exp(-350.0/T)$	22

*Units - k : $(m^3\ kg\ mole^{-1})^{n-1} sec^{-1}$ where n is reaction order
T : ^oK

$$k_{-j} = \frac{k_j}{K_{cj}}$$

The reaction mechanism chosen for H_2/air combustion consists of 13 reactions involving 8 chemical species (H_2, O_2, OH, O, H, N_2, H_2O, and HO_2). These are shown in Table I. The mechanism consists of four propagation reactions, four recombination/dissociation reactions, and five reactions involving HO_2.

Numerical Procedure

The above system of equations was solved using an implicit finit difference approach. The above boundary layer equations, with the exception of the continuity equation, can be written in the following general form

$$2\xi f' \frac{\partial F}{\partial \xi} + \frac{\alpha_1}{\eta_e} \frac{\partial F}{\partial \eta} + \frac{\alpha_2}{\eta_e^2} \frac{\partial^2 F}{\partial \eta^2} = \alpha_3 \tag{19}$$

where F represents any dependent variable. Expressions for the α_i coefficients are given in Table II.

TABLE II

Coefficients in Governing Equation

F	α_1	α_2	α_3
u	$(V - \ell')$	-1	$\dfrac{eg\beta(T - T_\infty)}{U_\infty}$
h	$(V - \dfrac{\overline{c}'}{cp})$	$-\dfrac{\overline{c}}{cp}$	$\dfrac{1}{(\rho\mu)_\infty}\dfrac{\partial}{\partial\eta}\left[\dfrac{\rho}{cp}\sum_i(Le_i - 1)h_i\dfrac{\partial\sigma_i}{\partial\eta}\right]$
σ_i	$(V - b_i')$	$-b_i$	$\dfrac{e}{\rho}S_i$

Finite Difference Procedure

The boundary layer is divided into a grid of increments $\Delta\xi$ and $\Delta\eta$. Denoting current locations in the ξ and η directions by $\xi = n \cdot \Delta\xi$ and $\eta = m \cdot \Delta\eta$ the following finite difference expressions can be introduced

$$\frac{\partial F}{\partial \xi} = \frac{F_{m+1,n} - F_{m,n}}{\Delta\xi}$$

$$\frac{\partial F}{\partial \eta} = a_1 F_{m+1,n+1} + b_1 F_{m+1,n} + c_1 F_{m+1,n-1}$$

$$\frac{\partial^2 F}{\partial \eta^2} = a_2 F_{m+1,n+1} + b_2 F_{m+1,n} + c_2 F_{m+1,n-1}$$

where

$$a_1 = \Delta\eta_{n-1}/(\Delta\eta_n \cdot \Delta\eta_T)$$

$$b_1 = (\Delta\eta_n - \Delta\eta_{n-1})/(\Delta\eta_n \cdot \Delta\eta_{n-1})$$

$$c_1 = -\Delta\eta_n/(\Delta\eta_{n-1} \cdot \Delta\eta_T)$$

$$a_2 = 2/\Delta\eta_n \cdot \Delta\eta_T)$$

$$b_2 = -2/(\Delta\eta_n \cdot \Delta\eta_{n-1})$$

$$c_2 = 2/(\Delta\eta_{n-1} \cdot \Delta\eta_T)$$

$$\Delta\eta_T = \Delta\eta_n + \Delta\eta_{n-1}$$

$$\Delta\eta_n = \Delta\eta_{n+1} - \Delta\eta_n$$

Substituting the above expressions into Eq. (19) results in a set of implicit finite difference equations of the form

$$AF_{m+1,n+1} + BF_{m+1,n} + CF_{m+1,n} = D \tag{20}$$

where

$$A = \frac{\alpha_1 a_1}{\eta_e} + \frac{\alpha_2 \ a_2}{\eta_e^2}$$

$$B = \frac{\alpha_1 b_1}{\eta_e} + \frac{\alpha_2 b_2}{\eta_e^2} + \frac{2\xi_{m+1} f'}{2\xi}$$

$$C = \frac{\alpha_1 c_1}{\eta_e} + \frac{\alpha_2 c_2}{\eta_e^2}$$

$$D = \alpha_3 + \frac{2\xi_{m+1} f'}{\Delta\xi} f_{m,n} \quad .$$

The difference equations (20) and the boundary conditions form a system of equations of the tridiagonal type. Variables in the coeficients of Eq. (20) are evaluated at the known step. The transformed velocity V is obtained from the finite difference form of the continuity equation

0 0 0 0 4 9 0 0 8 9 7

$$V_{m+1,n} = V_{m+1,n-1} - \Delta\eta_{n-1}\left(\frac{m+1}{\Delta\xi} + \frac{1}{2}\right)\left(f'_{m+1,n} + f'_{m+1,n-1}\right)\eta_e$$
$$+ \Delta\eta_{n-1}\left(\frac{\xi m+1}{\Delta\xi} - \frac{1}{2}\right)\left(f'_{m,n} + f'_{m,n-1}\right)\eta_e \qquad (21)$$

When the source terms are linear or mildly nonlinear such a system can be solved quite easily using standard techniques. However, for the species conservation equations convergence problems are often encountered due to the strongly coupled and highly nonlinear kinetic source terms. The approach of the present investigation was to use a standard tridiagonal matrix solution algorithm for solving the hydrodynamic equations for conservation of mass and momentum. The procedure followed and the formalism are due largely to Blottner[10]. The coupled energy and species conservation equations are then solved using a computational scheme developed by Pratt [11]. The latter involves forming a set of Newton Raphson correction equations of the form

$$\sum_{j=1}^{N}\left(\frac{\partial f_i}{\partial x_j}\right)\Delta x_j = -f_i \quad , \; i = 1,N$$

for an N dimensional system of equations f_i and unknowns x_j. Δx_j represent a set of correction variables. The dependent variables in the present case are the temperature, T, the inverse molecular weight, σ_m, and the species mole numbers, σ_i. The above system of equations is solved interatively by pivotal Gausian elimination for

the simultaneous determination of all the thermochemical variables across a particular grid row.

In the present scheme the boundary layer grid can be either uniform or allowed to vary across the boundary layer. For the case of a nonuniform grid, $\Delta\eta$ is calculated from the following expression

$$\Delta\eta_{N=1} \frac{k - 1}{(k^{NMAX-1} - 1)} \; ; \quad \Delta\eta_N = \Delta\eta_{N-1} \cdot k \tag{22}$$

Eq. (20) is second order accurate in the η direction and first order accurate in the streamwise direction. For the results presented here 40 points across the boundary layer between $\eta = 0$ and $\eta_e = 9.0$ where found to be sufficient. To improve accuracy near the wall where the steepest gradients occur a nonuniform grid was used with $\Delta\eta$ given by Eq. (21) with $k = 1.07$. Since the procedure is first order accurate in the streamwise direction, the solution is quite sensitive to step size in this direction. Thus, step size in the streamwise direction, $\Delta\xi$, was adjusted continuously to meet the desired accuracy of 5%. Minimum step size corresponded to a time step on the order of 10^{-7} sec.

At the plate leading edge ($\xi = 0$) the partial differential equations become ordinary differential equations in the transformed coordinate system and can be solved using the same procedure as is employed for the partial differential equations. In this case, however, the species source terms are set equal to zero. This solution thus provides the initial profile to start the solution along the plate surface.

RESULTS AND DISCUSSION

Noncatalytic Heated Plate

The results of the numerical calculations for the case of H_2/air flow over a heated plate with combustion at an equivalence ratio of 0.1 are shown in Figs. 1-4. In the case presented the wall temperature was assumed constant at $1100^{o}K$. The free stream velocity and temperature were 3.17m/s and $293^{o}K$ respectively. Boundary layer velocity profiles (normalized by the free stream velocity) are shown in Fig. 1 for distances of 2, 4, and 6 mm downstream of the plate leading edge. The velocity profiles are nearly similar both upstream and downstream of the combustion zone showing little effect of combustion on the profiles. This result is in agreement with that found by Peters[13] in a laminar flat plate boundary layer diffusion flame study.

Temperature profiles are plotted against the nondimensional boundary layer coordinate η in Fig. 2 for distances of $x = 0.60$, 1.89, 2.00, and 2.80 mm downstream of the plate leading edge. The temperature profiles are seen to remain similar until a distance of approximately 0.6 mm along the plate. Prior to this point little heat release due to chemical reaction has occurred. At $x = 1.89$ mm combustion has occurred near the wall as can be seen by the peak in the temperature profile. A short distance downstream ($x = 2.00$ mm) significant combustion has occurred, with the temperature reaching a maximum

of $1470^{o}K$. The combustion has also spread farther out into the boundary layer. At $x = 2.80$ mm the heat release rate due to combustion has decreased in regions near the wall and heat transfer has resulted in cooling of the hot combustion gases near the wall. Combustion of incoming reactants continues to occur farther out in the boundary layer but at a decreasing rate due to the lower temperatures.

Energy release rates are shown as a function of η in Fig. 3 for a distance of 2 mm downstream of the plate leading edge. The resulting increase in temperature can be seen in the corresponding curve of Fig. 2. Negative values correspond to a net energy release. It can be seen that the primary energy release reactions are the bi-molecular reaction

$$H_2 + OH \rightleftarrows H_2O + H \tag{2f}$$

due to its large forward rate at this point in the combustion zone, and the three body recombination reaction

$$H + O_2 + M \rightleftarrows HO_2 + M \tag{8f}$$

It is noteworthy that the HO_2 destruction reactions 9 through 13 also contribute significantly to the overall energy release mechanism. The importance of the HO_2 system in energy release was also noted by Miller and Kee[14] in a numerical study of a hydrogen-air laminar diffusion flame. Of the three-body recombination reactions which

typically dominate the energy release in many combustion systems, only the reaction

$$H + OH + M \rightleftarrows H_2O + M \qquad (6f)$$

contributes in the present case.

Species concentration profiles for several distances downstream from the plate leading edge are presented in Figs. 4-6. Profiles at x = 1.35 mm correspond to the induction period before any heat release due to chemical reaction that has occurred. O, H, OH, and HO_2 radical concentrations are rapidly increasing in the high temperature region near the heated wall. The H_2O concentration, while comparable to the radical concentrations, is still quite low. The H_2 has undergone little reaction at this point.

At x = 1.89 mm a small amount of chemical heat release has occurred near the wall (see corresponding temperature profile in Fig. 5). This release corresponds to the reaction of H_2 and O_2 near the wall, and the formation of relatively large amounts of H_2O. Radical concentrations of H, O, and OH have attained their peak values near the wall and are beginning to decrease as recombination reactions become important.

At x = 1.98 mm the reaction of H_2 and O_2 is apparent much farther out into the boundary layer. Concentrations of O, H, and OH continue to decrease immediately adjacent to the wall. A region can be seen

to exist away from the wall which is characterized by more intense heat release rates and high radical concentrations. However, due to the lower temperatures encountered here, heat release rates and maximum radical concentrations have decreased below those values found upstream and closer to the plate. Farther downstream this zone continues to exist but at increasingly greater distances from the wall.

The high concentrations of H_2O near the wall are, at first, surprising since these levels are a factor of 2 greater than the corresponding local equilibrium values. This is a consequence of the rapid diffusion rates of H_2 into the region near the wall. Fig. 7 presents calculated local diffusion velocities of various species across the boundary layer at x = 1.98 mm. Negative values of diffusion velocity indicate diffusion toward the wall. It can be seen that the diffusion velocity for H_2 is approximately a factor of 4 greater than other molecular species. A flux balance was carried out at several points across the boundary layer to verify the accuracy of the numerical calculations. The results indicated that O and H atoms are conserved. In addition, previous calculations carried out with a Lewis number of unity for all species indicated no such buildup of H_2O above its equilibrium concentration. Thus, it appears that the observed behavior of H_2O is attributable to rapid diffusion of low

molecular weight H_2 into the high temperature wall region, followed by the rapid conversion of H_2 to H_2O via reaction 2

$$H_2 + OH \rightleftarrows H_2O + H \qquad (2f)$$

A better understanding of the above species concentration profiles can be obtained by a more detailed examination of the reaction mechanism during the combustion process. Referring to Table II the primary reaction responsible for the initiation of chemical reaction is the reverse of reaction 13, i.e.,

$$H_2 + O_2 \rightleftarrows HO_2 + H \qquad (13r)$$

Once initiation has occurred, reaction (13) rapidly losses its importance and the following bimolecular branching reactions control the observed radical concentration buildup

$$H + O_2 \rightleftarrows O + OH \qquad (3f)$$

$$H_2 + OH \rightleftarrows H_2O + OH \qquad (2f)$$

$$O + H_2 \rightleftarrows OH + H \qquad (1f)$$

In addition, the rapid increase in HO_2 is due primarily to the three body reaction

$$H + O_2 + M \rightleftarrows HO_2 + M \qquad (8f)$$

As one moves downstream, at x = 1.90 mm, the bimolecular reactions (1), (2) and (3), approach partial equilibrium, along with reaction (4).

$$OH + OH \rightleftarrows H_2O + O \qquad (4)$$

The three body recombination reactions

$$H + OH + M \rightleftarrows H_2O + M \qquad (6)$$

$$H + H + M \rightleftarrows H_2 + M \qquad (5r)$$

$$O + O + M \rightleftarrows O_2 + M \qquad (7f)$$

become important in the removal of H, O, and OH, while reactions (9) through (13) result in the destruction of HO_2

$$HO_2 + H \rightleftarrows OH + OH \qquad (9f)$$

$$HO_2 + OH \rightleftarrows H_2O + O_2 \qquad (10f)$$

$$HO_2 + O \rightleftarrows OH + O_2 \qquad (11f)$$

$$HO_2 + H \rightleftarrows H_2O + O \qquad (12f)$$

$$HO_2 + H \rightleftarrows H_2 + O_2 \qquad (13f)$$

The above HO_2 destruction reactions also account for the minimums observed in the HO_2 profiles of Figs. 5 through 8. It can be seen that these minimums correspond to high levels of H, O, and OH radicals.

A comparison between predicted and experimental hydrodynamic boundary layer thickness is shown in Fig. 14 of the companion paper[5] for an experimentally measured wall temperature profile (average temperature of 1100 K) and a freestream velocity of 3.17 m/s. In both cases an

increase occurs in boundary layer thickness over that expected without combustion due to the high heat release associated with the onset of combustion. However, the predicted increase in thickness is much more abrupt, and occurs farther upstream (approximately 2 mm downstream from the leading edge) than is found experimentally. The latter doesn't become apparent until nearly 10 mm downstream from the leading edge.

Since good agreement was obtained between predicted and experimental results when no combustion is present, it would appear that the discrepancy in boundary layer thickness is due to the kinetic mechanism employed in the model. It is difficult to determine at this time which reaction rates are the primary cause of the discrepancy since the occurrence of combustion is a function of both the initial radical buildup rate and energy release rates in the primary combustion zone. As discussed above the initial radical buildup is controlled by the bimolecular branching reactions (1), (2), and (3), whereas energy release is due primarily to reactions (2) and (8). Rates for the bimolecular branching reactions are relatively well known, for the most part to within 30%. Expected uncertainty in rates for the three body recombination reactions (except for reaction (8) involving HO_2) is somewhat greater, but these reactions were found to be relatively unimportant to the combustion process. The greatest uncertainty in

the present kinetic mechanism appears to exist in the HO_2 reactions, the two most important being reactions (8f) and (13r). An examination of reaction rates during the induction period indicates that reaction (13r) is quite rapid relative to the other reactions and results in high H atom levels prior to the combustion zone. These high H atom levels, combined with the uncertainty in the rate constant for reaction (13), could account for the high energy release rates observed for the latter reaction (see Fig. 3). These comments are somewhat speculative at this time, and a more detailed examination of the reaction mechanism is needed before a definite conclusion can be drawn.

Catalytic Heated Plate

While the general role of a catalyst in promoting chemical reaction is well known, there is considerable uncertainty in many systems concerning the kinetic mechanism involved. This is particularly true at the high temperatures and pressures encountered in combustion systems. In the case of H_2 oxidation over platinum catalysts the results of low pressure studies have led to several possible mechanisms. Bond[14] favors a Langmuir-Hirshelwood mechanism for d-metals such as platinum which involves the adsorption of both H_2 and O_2 as follows:

$$H_2 + 2^* \rightarrow 2\underset{*}{H}$$

$$O_2 + 2^* \rightarrow \underset{*}{O} - \underset{*}{O}$$

$$2\underset{*}{H} + \underset{*}{O} - \underset{*}{O} \rightarrow 2\underset{*}{OH} + 2*$$

$$2\underset{*}{OH} + 2\underset{*}{H} \rightarrow 2H_2O + 4*$$

Here the * denotes bonding with a surface atom. In more recent work Netzer and Kneringer[15] found in a study of H_2 oxidation on a Pt(100) surface at low pressures ($\sim 10^{-8}$ torr) the existance of three temperature regions. Up to a surface temperature of 420 K both reactants are adsorbed on the surface and experimental results favor a reaction mechanism of the above type. Between 420°K and 770 K hydrogen tends to desorb and only oxygen remains on the surface in an appreciable concentration. In this case an Eley-Rideal mechanism is the most probable in which reaction takes place between adsorbed oxygen and H_2. Above 770 K neither reactant is adsorbed to an appreciable extent and the reaction rate is determined by the lifetime and collision frequency at the surface.

While it is difficult to extend the above results to conditions encountered in catalytic combustion, several general observations can be made. A number of intermediate species exist in bound surface states during H_2 oxidation. In the above mechanism these include H, O, and OH radicals. Since desorption is endothermic, a significant percentage of these intermediate surface species could be expected to desorb at high temperatures before surface reaction to H_2O could occur. Thus, in the present system, the surface could act to initiate radicals which diffuse out into the gas phase where homogeneous reac-

tions occur, or reaction can proceed entirely at the surface as in the above mechanism. It should be noted, however, that if radical initiation is important at the surface, then radical termination will also be important. The surface can never give radical concentrations greater than the equilibrium value.

In formulating a model for the present system the role of the catalyst must be considered. As is stated by Benson[17],

> "Its role is restricted to one of accelerating the rate of approach to equilibrium. However, in most chemical systems, there are many unstable compositions intermediate in free energy between reactants and the state of ultimate equilibrium. We can describe the 'specificity' of catalysts in terms of their property of accelerating the rate of approach to one of these intermediate states rather than a general, over-all acceleration toward the lowest state."

It has also been pointed out by Pfefferle and Carrubba[2] that at elevated temperatures and pressures, the rate of surface reaction becomes rapid relative to the rate of diffusion of species into and away from the surface. Under these conditions surface reactions are essentially diffusion limited. Based on the above considerations, one can then visualize as a limiting case an equilibrium wall condition.[10] In this case the catalytic wall is replaced by the condition that gas immediately adjacent to the wall is in equilibrium at a temperature corresponding to the wall temperature. While this is in keeping with the above mentioned role of a catalyst as accelerating the rates of approach of a system to equilibrium, a shortcoming is apparent in that it is unlikely a catalyst would be sufficiently non-selective so as to drive the system toward total equilibrium.

The corresponding boundary condition for the numerical calculations must meet two criteria. First, species concentrations must be those corresponding to an equilibrium composition. This equilibrium is determined by both the local wall temperature and the local composition. It is important to note that the latter is determined by the local relative diffusion rates of species into the wall, and thus can vary with distance along the plate. The second criteria is that the net flux of any element j must vanish at the wall. In the present case this can be written as

$$\sum_i \beta_i^j j_i = 0 \qquad i = 1,2...NS \tag{23}$$

where β_i^j is the amount of element j in species i, and j_i is the flux of specie i in a direction normal to the wall. Since the velocity is zero at the wall, j_i is the flux due to diffusion, and Eq. (23) relates the concentration gradients of the various species at the wall. Since there are two elements involved in chemical reactions, O and H, Eq. (23) provides 2 equations for the 8 unknown wall concentrations σ_i. Five additional equations are provided by the equilibrium relations

$$\frac{\sigma_{OH}}{\sigma_{O_2}^{\frac{1}{2}} \sigma_{H_2}^{\frac{1}{2}}} = K_1 \quad ; \quad \frac{\sigma_H}{\sigma_{H_2}^{\frac{1}{2}}} = K_2$$

$$\frac{\sigma_O}{\sigma_{O_2}^{\frac{1}{2}}} = K_3 \quad ; \quad \frac{\sigma_{HO_2}}{\sigma_{H_2}^{\frac{1}{2}}\sigma_{O_2}} = K_4$$

$$\frac{H_2O}{\sigma_{H_2}\sigma_{O_2}^{\frac{1}{2}}} = K_5 \tag{25}$$

where K_i is the equilibrium constant based on species mole numbers. Since N_2 undergoes no reactions, the final equation is provided by the condition

$$\left.\frac{\partial\sigma_{N_2}}{\partial y}\right|_{wall} = 0 \tag{25}$$

Using the above boundary conditions, calculations were carried out for the same conditions as in the previous section for a non-catalytic wall with combustion. OH concentration profiles as a function of η are shown in Fig. 8 for several distances downstream of the leading edge. For distances less than 0.5 mm from the leading edge the profiles are approximately similar. In this region convection and diffusion are of primary importance due to the large gradients existing near the leading edge. As a result, no concentration build-up occurs in the boundary layer due to homogeneous reactions. At $x = 2.0$ mm the boundary layer has become thicker with a resulting decrease in convective and diffusive rates. At this point the generation of OH due to homogeneous reaction is sufficient to cause an increase

in OH in the boundary layer, and the surface becomes a sink instead of a source of radicals. As one moves downstream, peak levels of OH increase, and the maximum concentrations occur farther out in the boundary layer. Note however, due to the low equilibrium radical concentrations maintained at the wall, peak levels are an order of magnitude less than were found with the noncatalytic wall.

Typical H_2 and H_2O profiles are shown in Fig. 9. Once again the profiles are approximately similar up to a distance of 0.5 mm from the leading edge. At $x = 4.4$ mm a small amount of gas phase reaction is apparent as a reduction of H_2 in the boundary layer and a slight increase in H_2O. At $x = 6.3$ mm and 7.8 mm combustion is occurring farther into the boundary layer with a significant decrease and corresponding increase in H_2O. The corresponding temperature profiles are shown in Fig. 10. Profiles up to 4.4 mm from the leading edge are similar as expected and indicate the occurrence of little heat release. Downstream of this location, increased homogeneous combustion occurrs with a resulting increase in boundary layer temperature. However, combustion and heat release rates are significantly lower than those found with a noncatalytic wall.

In summary, the equilibrium wall acts as a source of radicals near the plate leading edge, and a sink for radicals farther downstream. Because of the thin boundary layer, radical buildup in

the boundary layer near the leading edge is limited by rapid diffusion and convection. Downstream of this initial region, the rapid combustion and heat release rates found in the case with a noncatalytic wall are surpressed by the low radical concentrations existing in high temperature regions near the wall due to the equilibrium wall condition. With an equilibrium wall significant gas phase reaction and heat release did not occur until approximately 4.4 mm downstream from the leading edge. With a noncatalytic wall the primary combustion zone occurred approximately 2 mm downstream from the leading edge. Since experimental results presented in the companion paper[5] indicate that the presence of a catalytic wall enhances the combustion process, it would appear that the model does not sufficiently account for catalytic wall reactions.

CONCLUSIONS

A computer program has been developed to solve the boundary layer equations for laminar flow over a heated flat plate with H_2/air combustion. A reaction mechanism which includes 13 reactions involving 8 chemical species has been adopted.

The numerical calculations indicate the existence of several stages of combustion for a lean ($\phi = 0.1$) H_2/air mixture over a heated constant temperature noncatalytic plate. An initial region

near the plate leading edge corresponds to an induction period during which radical concentrations increase with little associated heat release. In this region temperature and velocity profiles are approximately similar and the boundary layer thickness corresponds to that for no combustion. Farther downstream heat release rates become appreciable due to the reaction of H_2. The boundary layer rapidly thickens and gas temperatures greater than the wall temperature are achieved. H_2O levels up to a factor of 2 greater than local equilibrium values are also found to occur near the wall due to the rapid diffusion of H_2 from the outer boundary layer. Downstream of the primary combustion zone heat losses to the wall result in lower gas temperatures and the profiles again approach a similar solution.

A simplified model for a catalytic surface based on an equilibrium wall was formulated. Radical buildup and the initiation of combustion were limited near the plate leading edge by rapid diffusion and convection in the boundary layer. Farther downstream gas phase radical concentrations were surpressed by the low equilibrium wall concentrations. This resulted in a delay of the onset of homogeneous gas phase reactions and gave signifcantly lower heat release rates than were found for the case with a noncatalytic wall. Based on experimental results it appears that this equilibrium model does not sufficiently account for catalytic wall reactions.

REFERENCES

1. Blazowski, W.S. and Walsh, D.E., Combust. Sci. Technol. 10, 233 (1975).

2. Pfefferle, W.C., Carrubba, R.V., Heck, R.M. and Roberts, G.W., "Catathermal Combustion: A New Process for Low Emissions Fuel Conversion," ASME Paper 75-WA/FU-1 (Dec. 1975).

3. Anderson, D.N. Tacina, R.R., and Mroz, T.S., "Performance of a Catalytic Reactor at Simulated Gas Turbine Combustor Operating Conditions", NASA TMX-71747 (June 1975).

4. Kesselring, J.P., Brown, R.A., Schreiber, R.J., and Moyer, C.B., "Catalytic Oxidation of Fuels for NO_x Control from Area Sources".

5. Robben, R.A., Schefer, R.W., Namer, I., and Agrawal, Y., "Catalytic Combustion in a Flat Plate Boundary Layer. I. Experimental Measurements and Comparisons with Numerical Calculations", to be presented at the Fall meeting, Western States Section/The Combustion Institute, Stanford University, Stanford, CA (1977).

6. Fristram, R.M. and Westenberg, A.A., "Molecular Transport Properties for Flame Studies", Fire Research Abstracts and Reviews, 8, 3 (1966).

7. Bird, R.B., Stewart, W.E., and Lightfoot, E.N., Transport Phenomena, John Wiley and Sons, New York (1960).

8. Hirshchfelder, J.O., Curtiss, C.F., and Bird, R.B., The Molecular Theory of Gases and Liquids, John Wiley and Sons, New York. (1954).

9. Gordon, S. and McBride, B., "Computer Program for Calculation of Complex Chemical Equilibrium Compositions", NASA SP-273 (1971).

10. Blottner, F.G., Johnson, M. and Ellis, M., "Chemically Reacting Viscous Flow Program for Multi-Component Gas Mixutres", Sandia Laboratories Report SC-RR-70-754 (1971).

11. Pratt, D.T., and Wormeck, J.J., "CREK - a Computer Program for Calculation of Combustion Reaction Equilibrium and Kinetics in Laminar or Turbulent Flow", Washington State University Report WSU-ME-TEL-76-1 (1976).

12. Peters, N., Int. J. Heat Mass Transfer, 19, 385 (1976).

13. Miller, J.A. and Kee, R.J., "Chemical Nonequilibrium Effects in Hydrogen-Air Laminar Jet Diffusion Flames", Sandia Laboratories Report SAND77-8505.

14. Bond, B.C., Catalysis by Metals, Academic Press, New York (1962).

15. Netzer, F.D. and Kneringer, G., Surface Sci. 51, pg. 526 (1975).

16. Benson, S.W., The Foundation of Chemical Kinetics, McGraw-Hill, New York (1960).

17. Baulch, D.L., Drysdale, D.D., and Horne, D.G., Fourteenth Symposium (International) on Combustion, The Combustion Institute, Pittsburgh, 107 (1973).

18. Wilson, W.E., Jr., J. Chem. Ref. Data 1, 535 (1972).

19. Baulch, D.L., Drysdale, D.D., Horne, D.G., and Lloyd, A.C., Evaluated Kinetic Data for High Temperature Reactions, Butterworths, London, Vol. 1 (1972).

20. Myerson, A.L. and Watt, W.D., J. Chem. Phys. 49, 425 (1968).

21. Johnston, H.S., "Gas Phase Reaction Kinetics of Neutral Oxygen Species," NSRDS-NBS 20 (1968).

22. Lloyd, A.C., Int. J. Chem. Kinetics 6, 169 (1974).

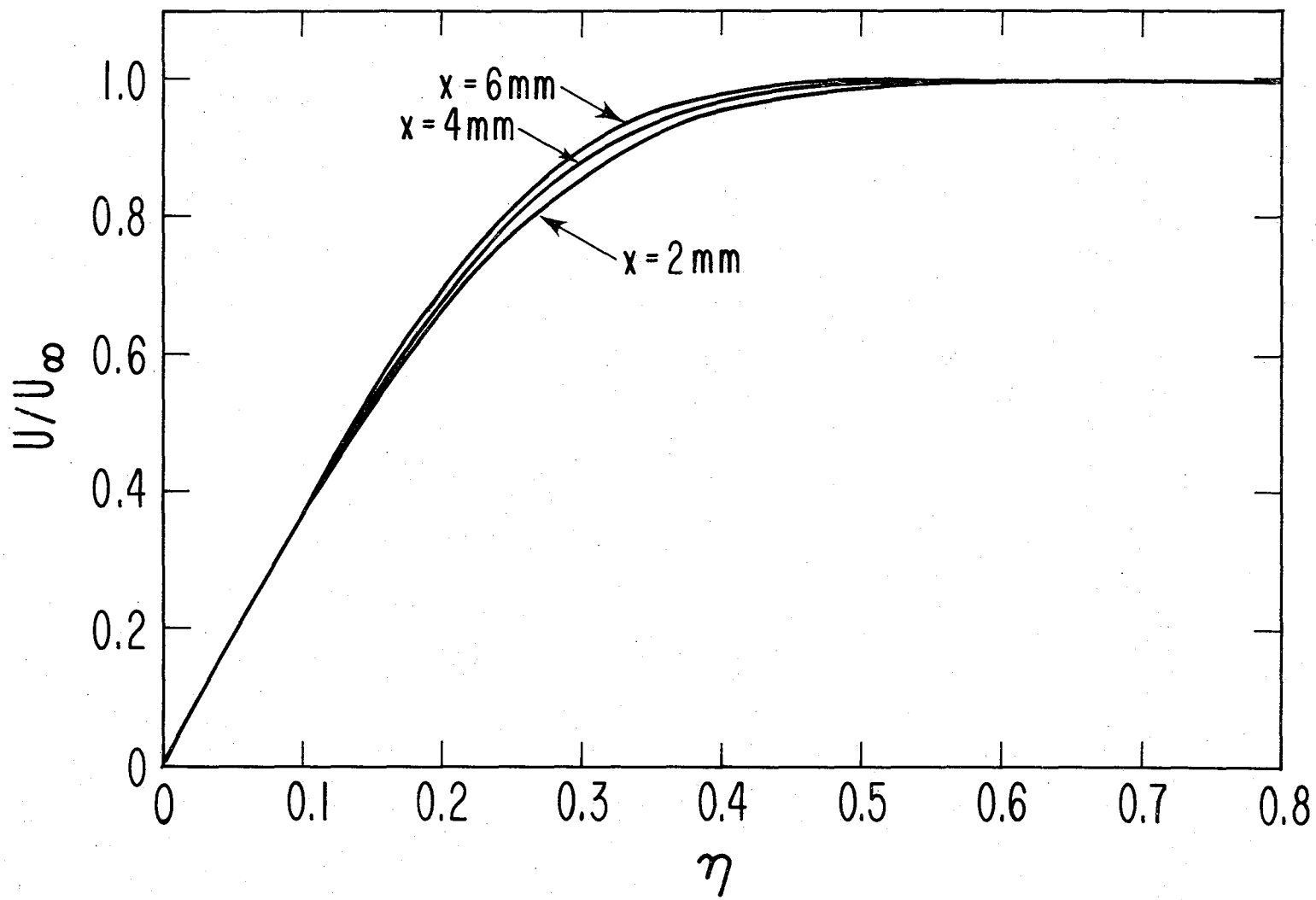

Figure 1. Normalized velocity profile as a function of nondimensional distance above plate for a noncatalytic plate. H_2/air combustion. $\phi = 0.1$, $T_{wall} = 1100K$, $U_\infty = 3.17$ m/s, $T_\infty = 293K$. XBL779-2004

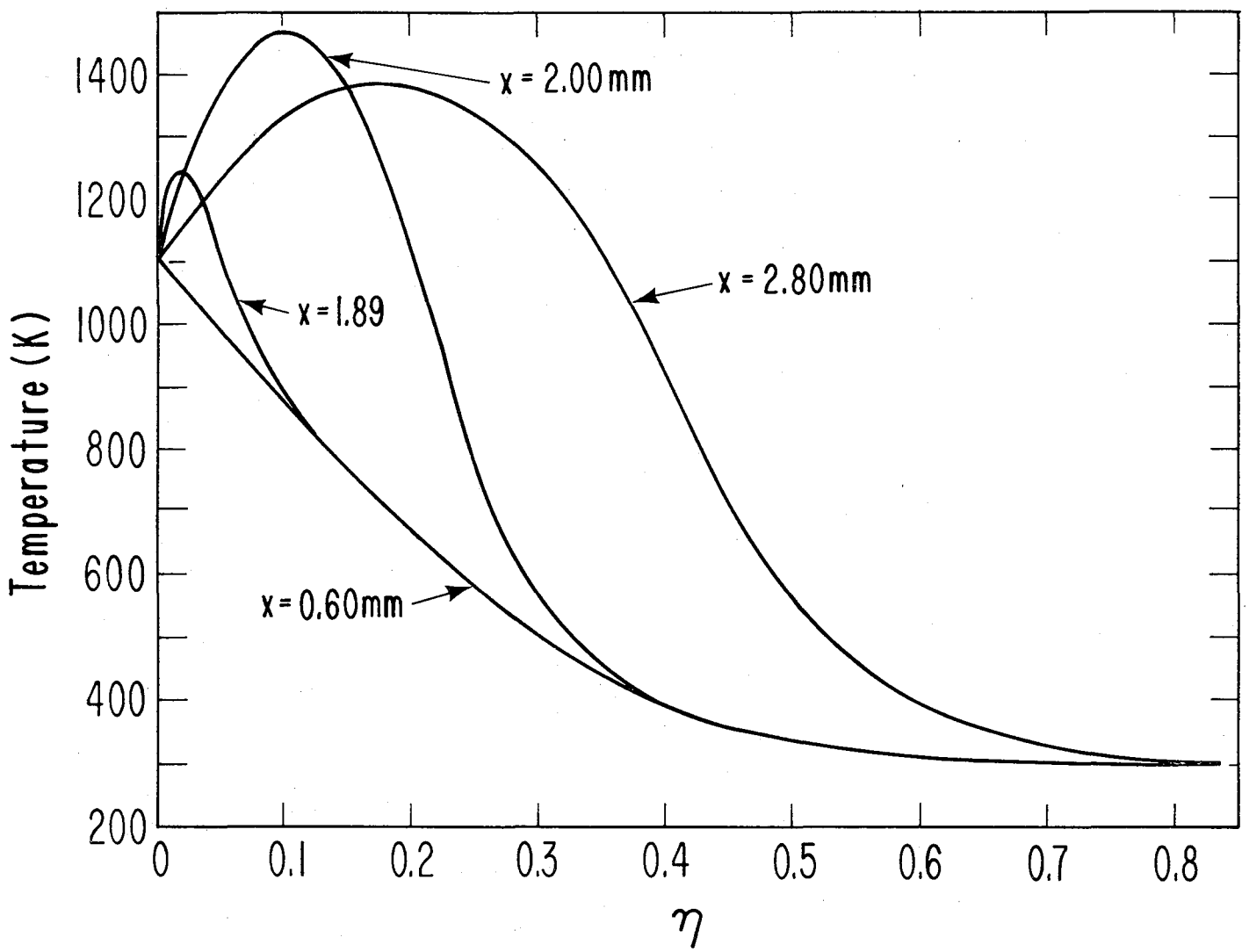

Figure 2. Boundary layer temperature distribution for a noncatalytic plate. XBL 779-2005
H_2/air combustion. $\phi = 0.1$, $T_{wall} = 1100K$, $U_\infty = 3.17$ m/s,
$T_\infty = 293K$.

0 0 0 4 9 0 0 7

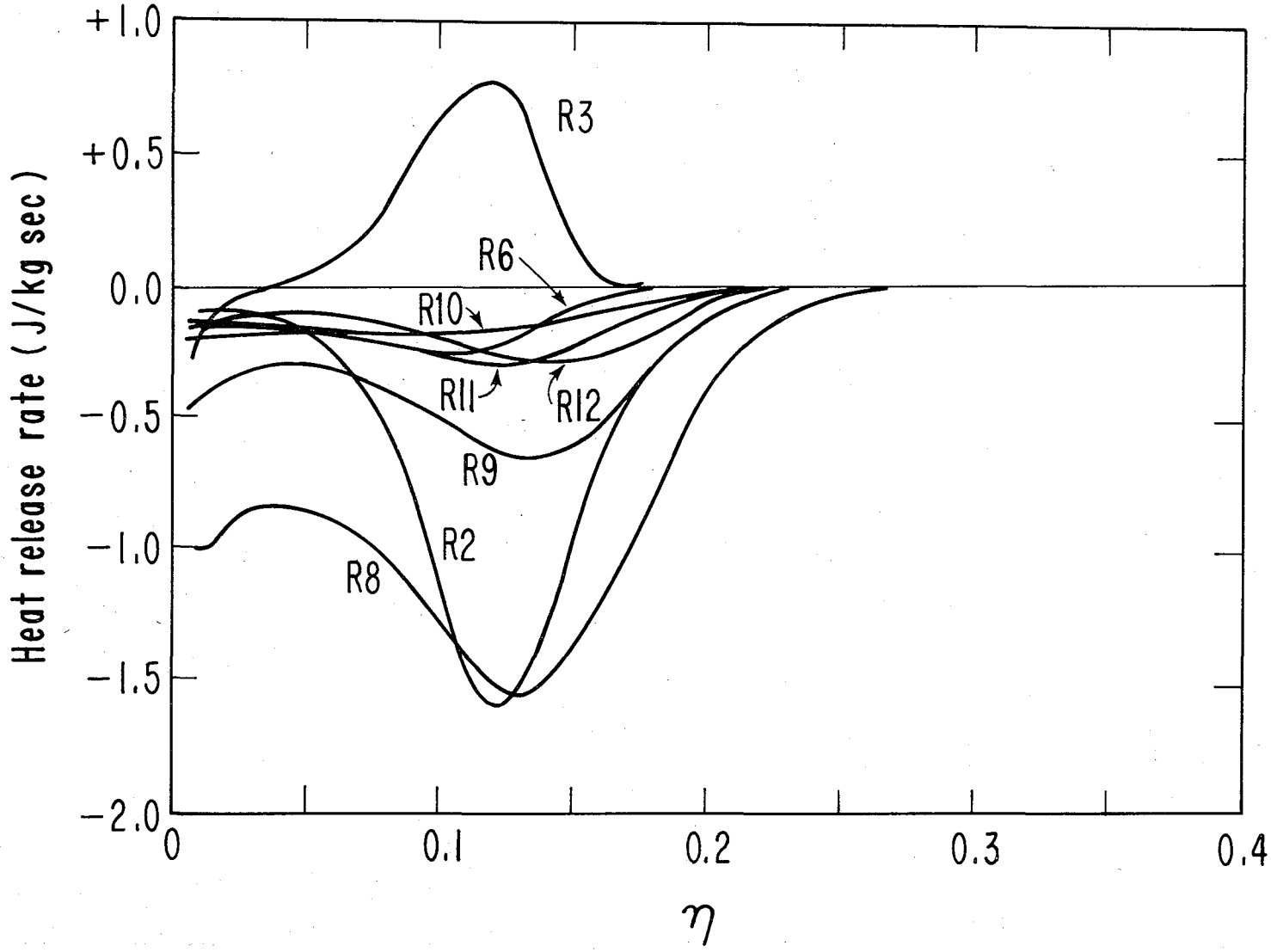

Figure 3. Energy release rates as a function of nondimensional distance above plate for a noncatalytic plate. x = 1.98 mm downstream from leading edge. H_2/air combustion. ϕ = 0.1, T_{wall} = 1100K, U_∞ = 3.17 m/s, T_∞ = 293K.

XBL 779-2013

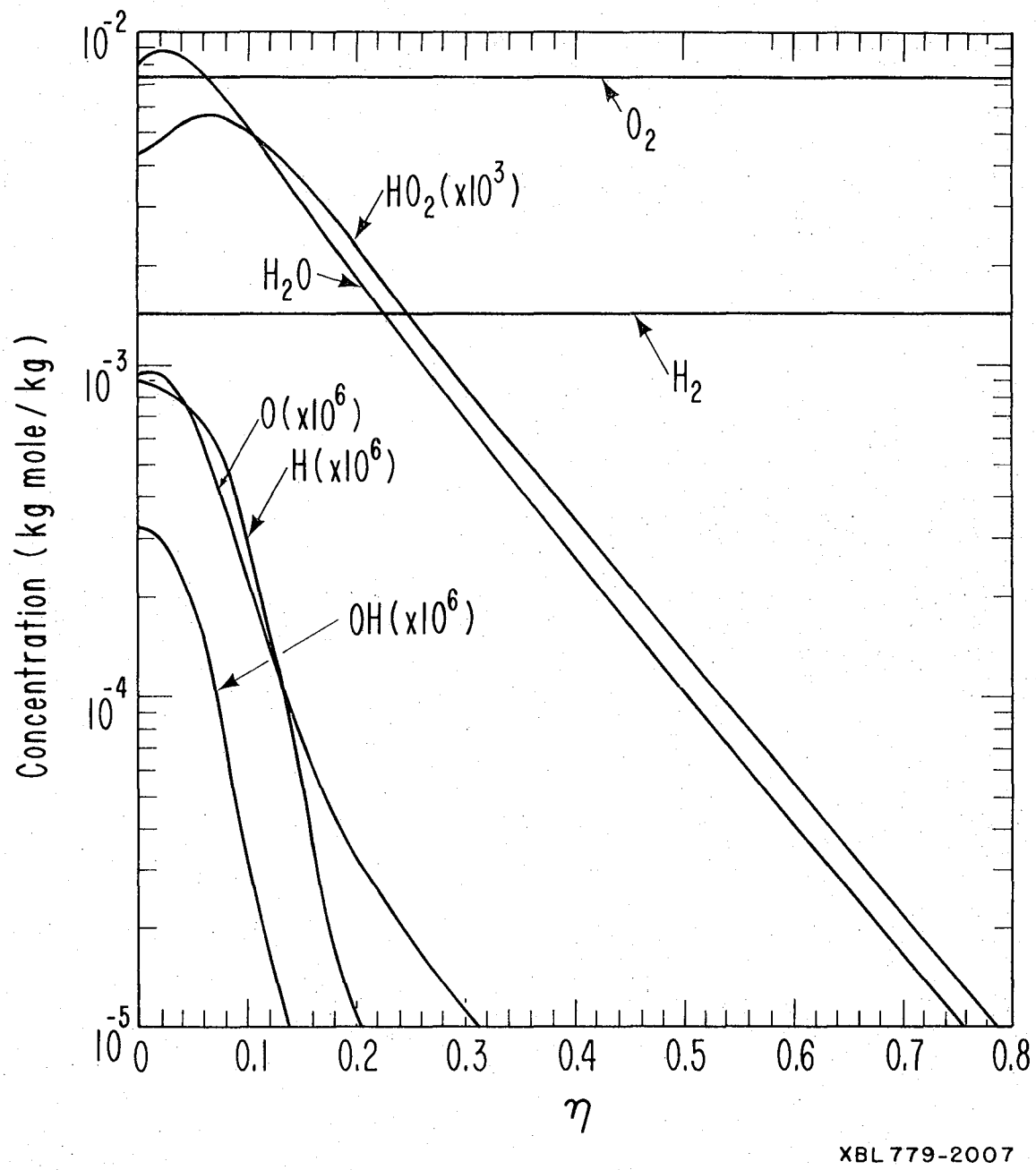

Figure 4. Concentration profiles as a function of nondimensional distance above plate for a noncatalytic plate. x = 1.35 mm downstream from leading edge. H_2/air combustion. ϕ = 0.10, T_{wall} = 1100K, U_∞ = 3.17 m/s.

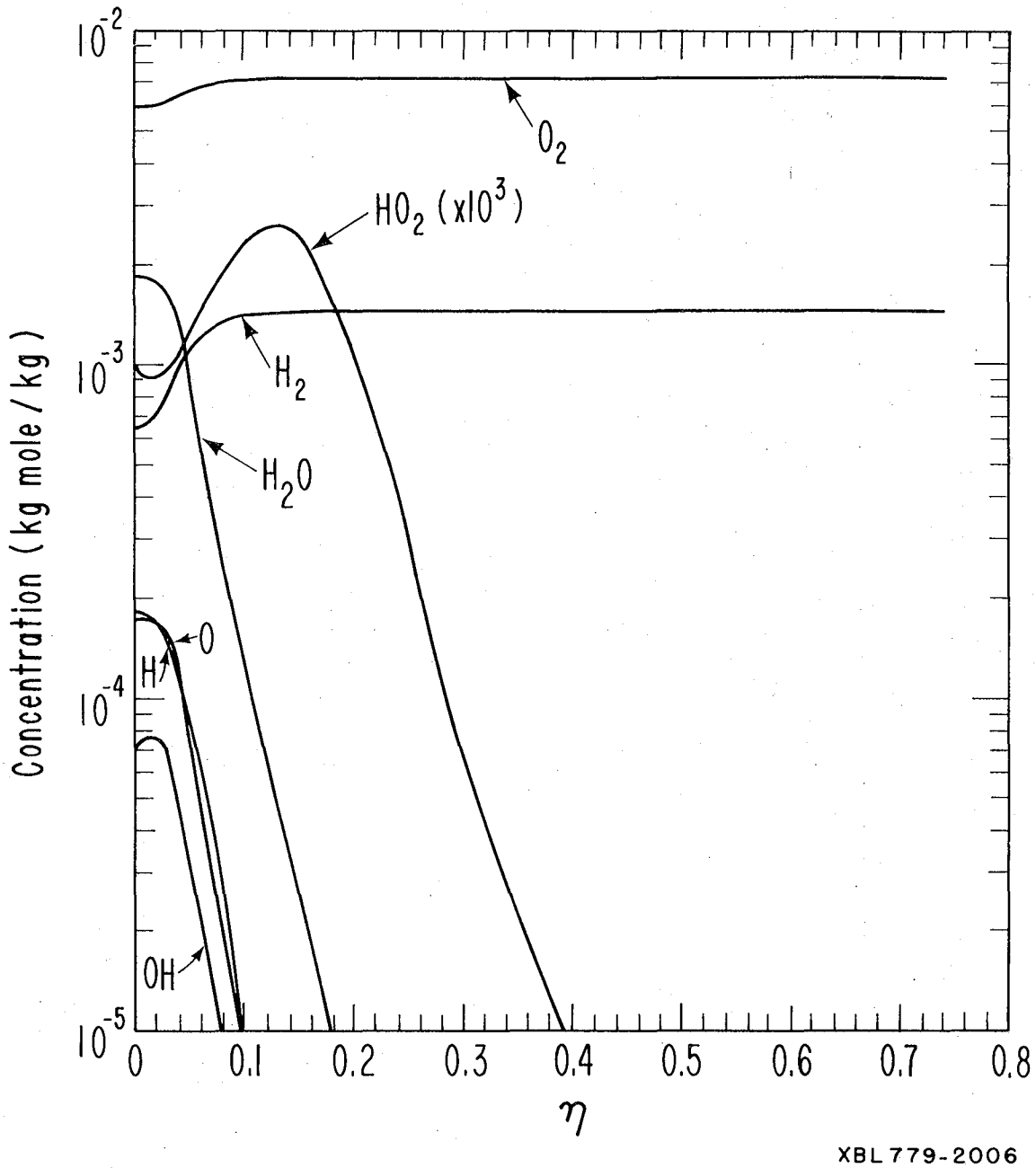

Figure 5. Concentration profiles as a function of nondimensional distance above plate for a noncatalytic plate. x = 1.89 mm from leading edge. H_2/air combustion. ϕ = 0.1, T_{wall} = 1100K, U_∞ = 3.17 m/s.

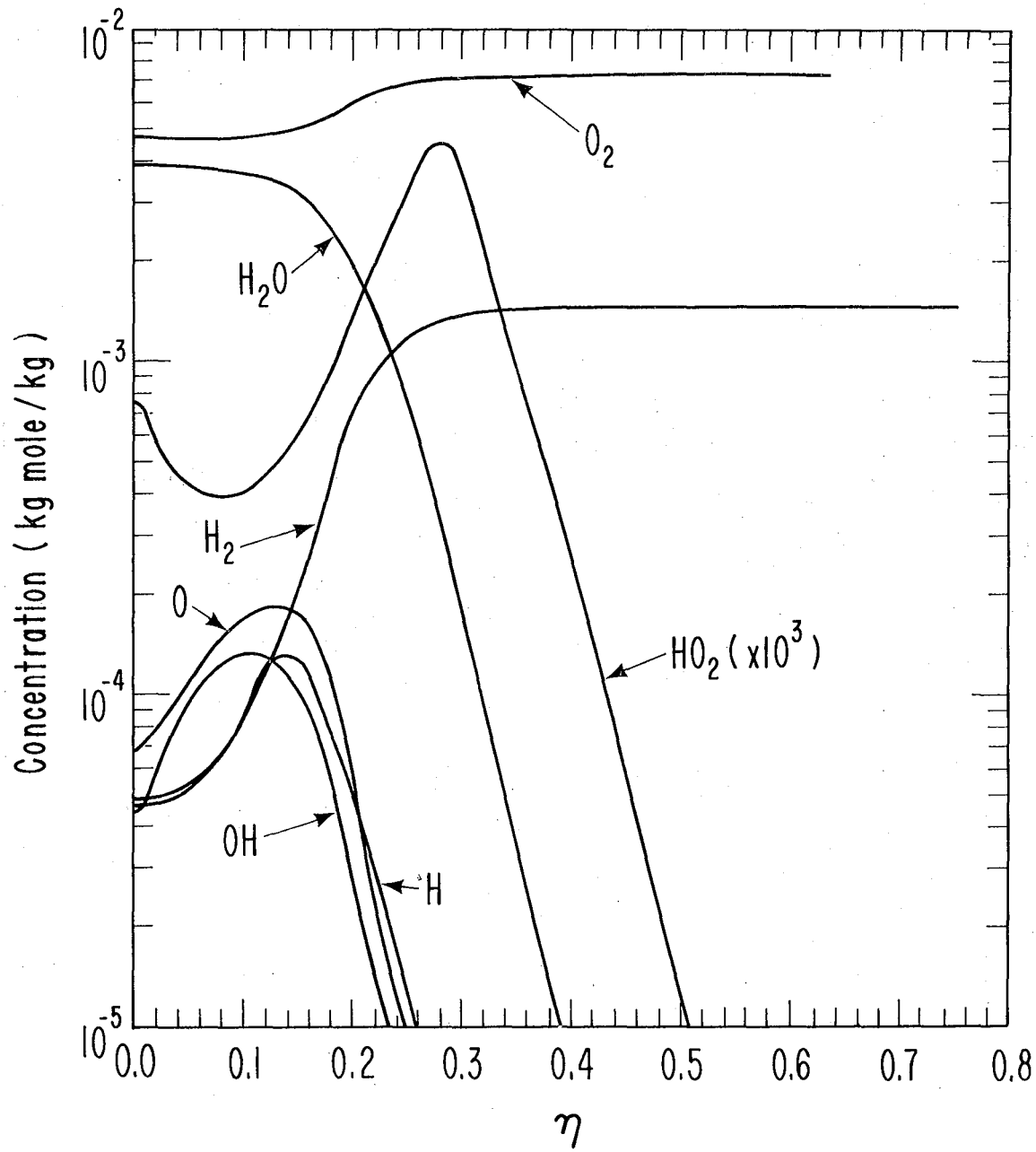

XBL 779-2008

Figure 6. Concentration profiles as a function of nondimensional distance above plate for a noncatalytic plate. x = 1.98 mm downstream from leading edge. H_2/air combustion. ϕ = 0.10, T_{wall} = 1100K; U_∞ = 3.17 m/s.

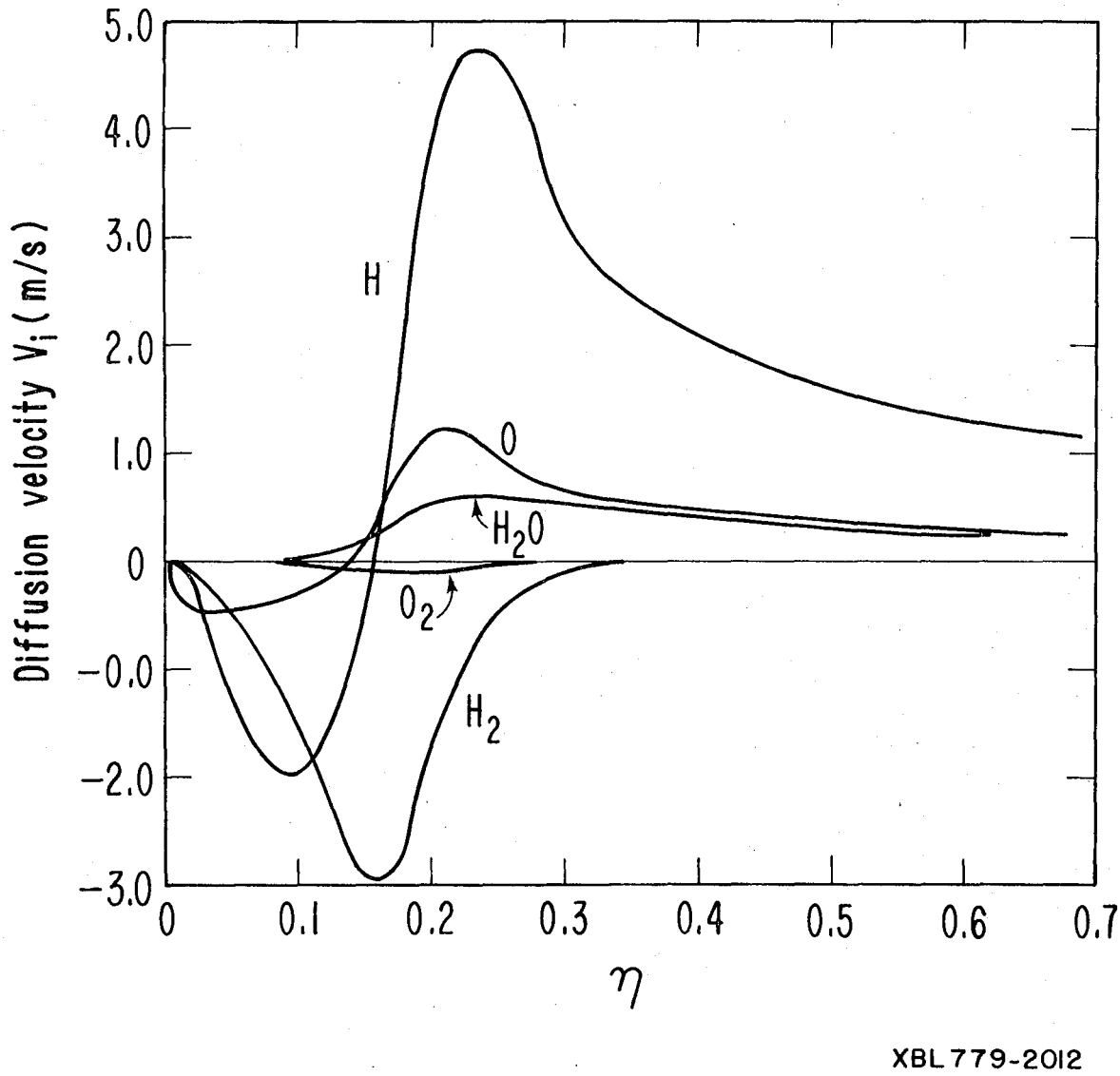

XBL 779-2012

Figure 7. Species diffusion velocites as a function of nondimensional distance above plate for a noncatalytic plate. x = 1.98 mm downstream of leading edge. H_2/air combustion. ϕ = 0.1, T_{wall} = 1100K, U_∞ = 3.17 m/s, T_∞ = 293K.

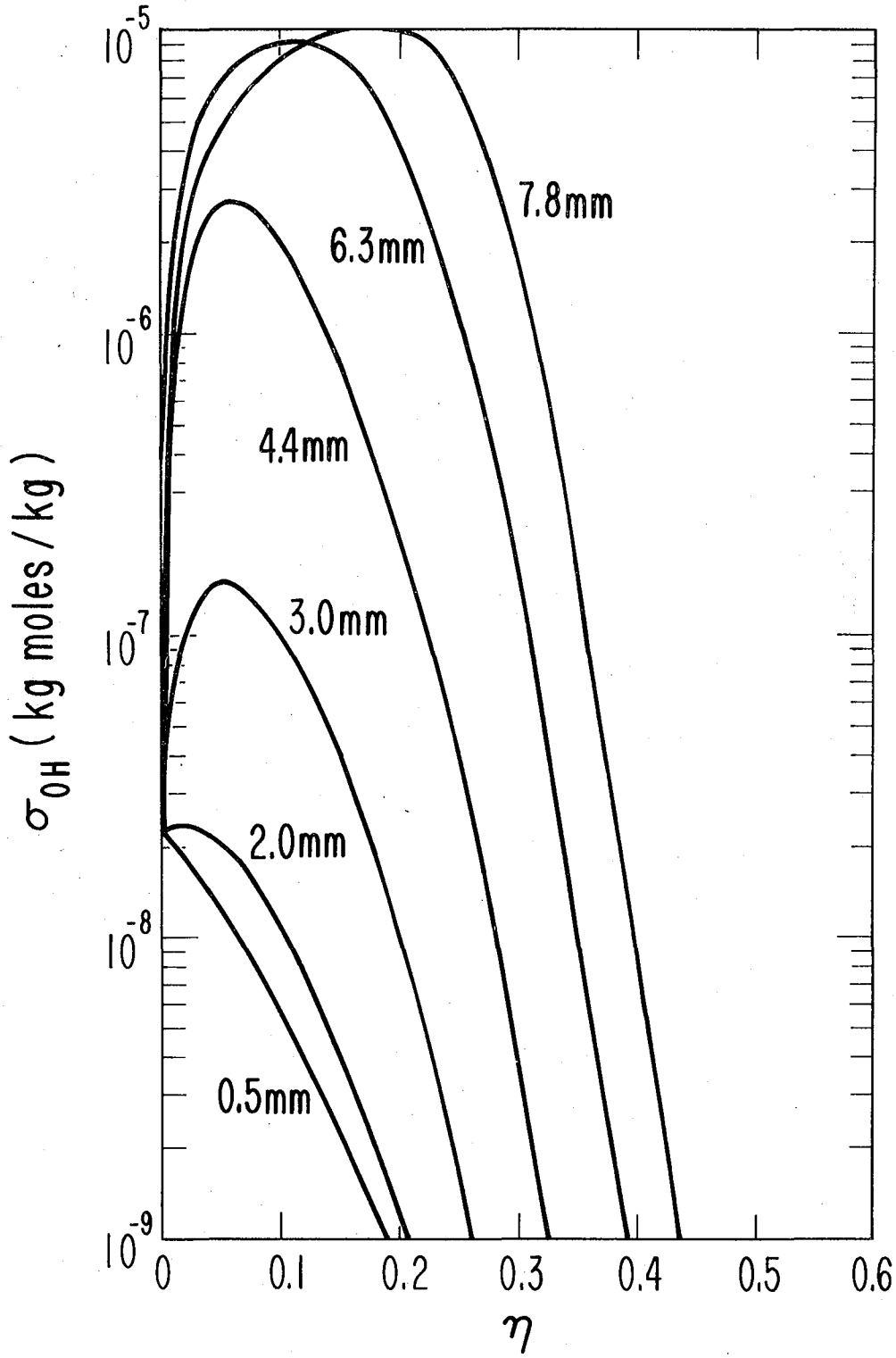

XBL7710-2045

Figure 8. OH concentration profile as a function of nondimensional distance above plate for a catalytic plate. Total equilibrium wall boundary condition. H_2/air combustion. $\phi = 0.1$, $T_{wall} = 1100K$, $U_\infty = 3.17$ m/s, $T_\infty = 293K$.

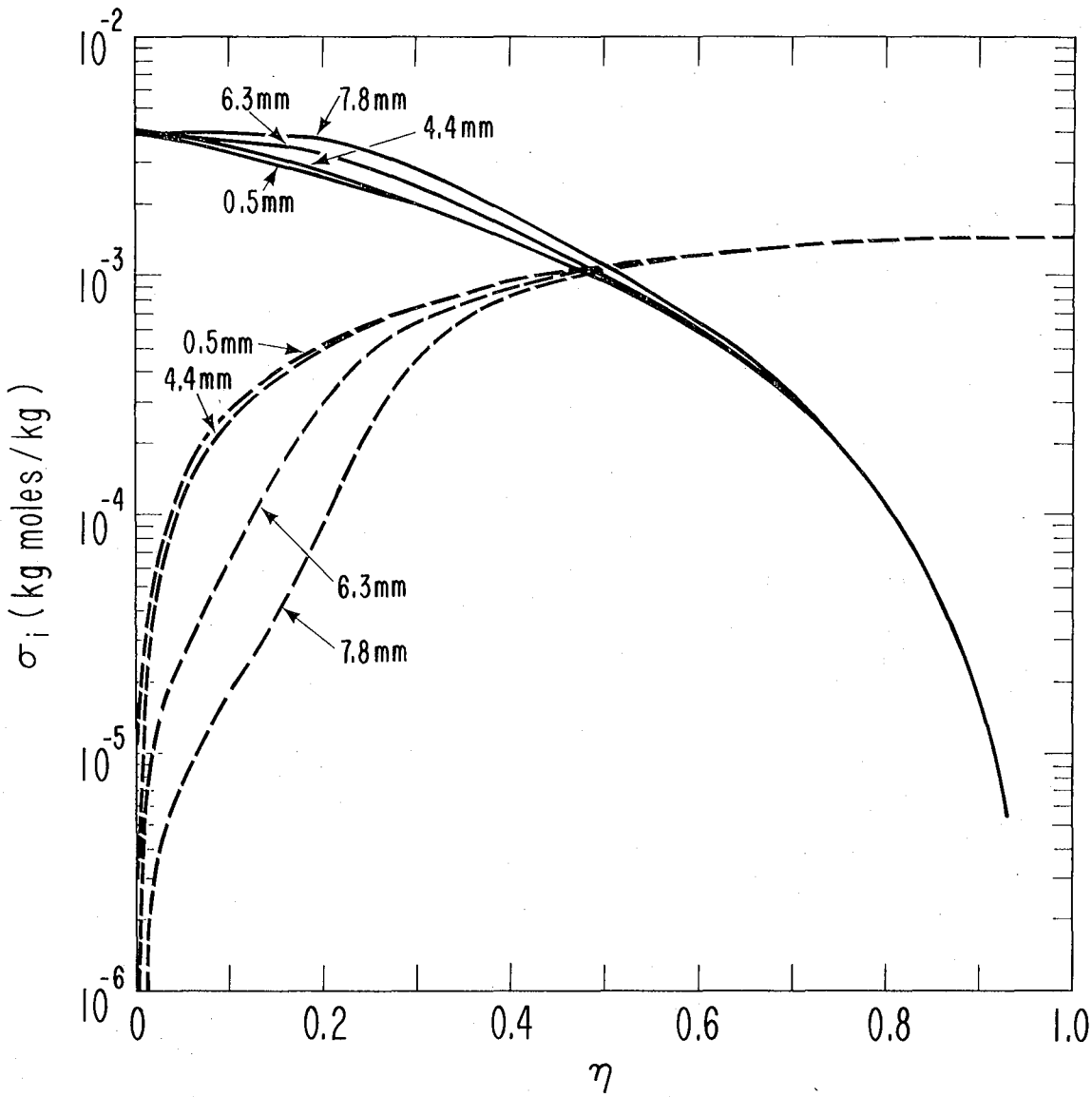

XBL7710-2046

Figure 9. H_2 and H_2O concentration profiles as a function of nondimensional distance above plate for a catalytic plate. Total equilibrium wall boundary condition. H_2/air combustion. ϕ = 0.1, T_{wall} = 1100K, U_∞ = 3.17 m/s, T_∞ 293K.

0 0 0 0 4 9 0 0 9 1 1

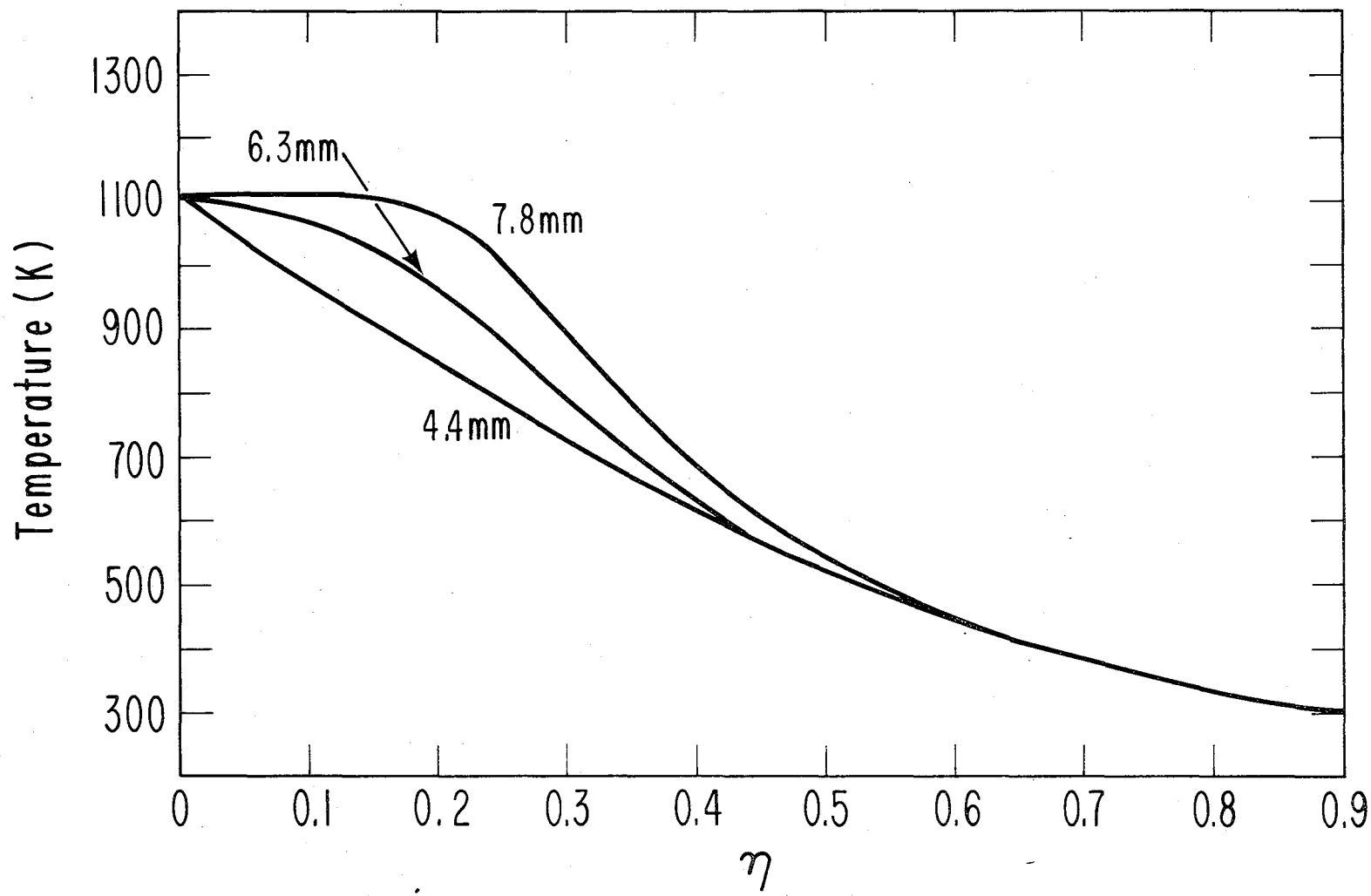

Figure 10. Boundary layer temperature distribution for a catalytic plate. XBL 7710-2044
Total equilibrium wall boundary condition. H_2/air combustion.
$\phi = 0.1$, $T_{wall} = 1100K$, $U_\infty = 3.17$ m/s, $T_\infty = 293K$.

This report was done with support from the United States Energy Research and Development Administration. Any conclusions or opinions expressed in this report represent solely those of the author(s) and not necessarily those of The Regents of the University of California, the Lawrence Berkeley Laboratory or the United States Energy Research and Development Administration.

0 0 0 0 4 5 0 2 2 9 4